Regulation of the EGF Transcriptional Response by Endocytic Sorting

Brankatschk, B ; Wichert, S P ; Johnson, S D ; Schaad, O ; Rossner, M J ; Gruenberg, J

Abstract: Ligand binding to the epidermal growth factor receptor (EGFR) on the cell surface activates the extracellular signal-regulated kinase (ERK) cascade. Activated, ligand-bound receptors are internalized, and this process may contribute to termination of signaling or enable signaling from intracellular sites. ESCRT (endosomal sorting complex required for transport) complexes may contribute to termination of signaling by sorting receptors into intraluminal vesicles of multivesicular endosomes from which the receptors continue into lysosomes for degradation. We showed that depletion of ESCRTs, which causes the retention of the EGFR in endosomes, increased the activation of the EGFR and its downstream kinases but had little effect on the overall profile and amplitude of the EGF-induced transcriptional response. In contrast, interfering with receptor endocytosis or ubiquitination to keep the EGFR at the cell surface stimulated increases in the abundance of many EGF-induced transcripts, similar to those induced by EGFR overexpression. We also found that the complete EGF transcriptional program was rapidly activated after ligand binding to the receptor. We conclude that the transcriptional response is elicited primarily by receptor molecules at the cell surface.

DOI: https://doi.org/10.1126/scisignal.2002351

Regulation of the EGF Transcriptional Response by Endocytic Sorting

Ben Brankatschk[1,*], Sven P. Wichert[2], Shem D. Johnson[1], Olivier Schaad[1,3], Moritz J. Rossner[2], and Jean Gruenberg[1, 4]

[1]Department of Biochemistry, University of Geneva, 30 Quai E. Ansermet, 1211 Geneva 4, Switzerland.

[2]Research Group Gene Expression, Max Planck Institute of Experimental Medicine, Hermann-Rein-Str. 3, 37075 Goettingen, Germany.

[3]Genomics platform, CMU, University of Geneva, 1 Rue Michel-Servet, 1211 Geneva 4, Switzerland.

[4]To whom correspondence should be addressed. Tel: +41-22-379.6464; fax: +41-22-379.6470; e-mail: jean.gruenberg@unige.ch.

[*]BB new address is: Research Group Gene Expression, Max Planck Institute of Experimental Medicine, Hermann-Rein-Str. 3, 37075 Goettingen, Germany.

ABSTRACT

Ligand binding to the epidermal growth factor receptor (EGFR) on the cell surface elicits activation of the extracellular signal-regulated kinase (ERK) mitogen-activated protein kinase (MAPK) cascade. Signaling is presumably terminated by both internalization and ESCRT (endosomal sorting complex required for transport)-dependent sorting of the receptor into intralumenal vesicles of multivesicular endosomes. Here, we showed that depletion of ESCRTs had little effect on the overall architecture and amplitude of the EGF response, whereas the abundance of some transcripts involved in nuclear factor κB and cytokine signaling increased. However, interfering with receptor endocytosis or ubiquitination stimulated increases in the abundance of many EGF-induced transcripts, similar to that induced by EGFR overexpression. We also found that the complete EGF transcriptional program was set in motion within a relatively short time period following ligand binding to the receptor. We conclude that the transcriptional response is elicited primarily by receptor molecules at the cell surface or by internalized EGFR cycling back to the plasma membrane.

INTRODUCTION

Like other signaling receptors, the epidermal growth factor (EGF) receptor (EGFR) is endocytosed upon stimulation with ligand and transported to lysosomes for degradation, thereby protecting cells from excess activation (1). After internalization, ubiquitinated EGFR molecules are incorporated into intralumenal vesicles of multivesicular endosomes (2-4), uncoupling the cytoplasmic domain from its signaling effectors in the cytosol. Intralumenal vesicles with their receptor cargo are then transported to lysosomes and degraded (5, 6). Sorting into intralumenal vesicles is controlled by CBL-mediated ubiquitination of the receptor cytoplasmic domain (7, 8). Ubiquitin molecules bind the clathrin adaptor HRS (hepatocyte growth factor-regulated tyrosine kinase substrate), a subunit of ESCRT-0 (endosomal sorting complex required for transport), which in turn recruits ESCRT-I, -II and -III, leading to receptor incorporation into intralumenal vesicles. ESCRTs couple receptor sorting with the membrane deformation and fission process (7, 9)

during the formation of intralumenal vesicles containing the EGFR (10). Conversely, EGF itself regulates the pathway, because addition of EGF increases the number of multivesicular endosomes that form in an ESCRT-dependent manner (11, 12).

Endocytic membrane traffic is also believed to orchestrate the signaling response (13-20). Clathrin-mediated endocytosis of the EGFR was proposed to control specific signaling pathways (21), or to be a prerequisite for EGF-dependent biological responses through receptor recycling (22). By contrast, a clathrin-independent pathway may target the receptor for degradation (22-24) at least in some cell types (25).

In contrast to other ligands, EGF remains receptor-bound in endosomes, whether EGFR is recycled (26) or is transported to lysosomes for degradation (1). Thus EGFR remains in principle signaling-competent, and endosomes indeed contain active EGFR and most components of the extracellular signal-regulated kinase (ERK) and mitogen-activated protein kinase (MAPK) (ERK/MAPK) cascade (13, 27). This may explain how some growth factors can elicit a complex, sometimes diverse, response through waves of compartmentalized signaling that are spatially and temporally regulated (14, 15, 17, 19, 28). This notion is further supported by the findings that a MAPK scaffold complex consisting of p14, MP1 (MEK partner 1) (29) and p18 (30) is present on late endosomes and required for full activity of the MAPK cascade. It is however not clear whether EGFR is itself part of this endosomal signaling complex, nor is it clear how the pool of active endosomal receptor is regulated and the extent to which it contributes to the biological response. Here, we have investigated how membrane traffic and receptor sorting along the endocytic pathway regulate the EGF-mediated transcriptional response.

RESULTS

Depletion of ESCRT subunits or VPS4A does not increase EGF signaling

To study the acute signaling response triggered by EGF in live cells over time, we used a reporter HeLa cell line that stably expresses the activator domain of ELK1 (a transcription factor downstream of ERK) and contains a luciferase expression cassette (HLR-ELK1) (31). Luciferase activity was measured in a light-tight incubator equipped for light detection. Addition of EGF increased luciferase activity (Fig. 1A) in a manner that was sensitive to tyrphostin (AG1478), which inhibits the tyrosine kinase activity of EGFR (32). The signal was reduced by EGFR knockdown to ≈20% (above background) of the mock-treated control (Fig. 1B), and could be increased to ≈250% by EGFR overexpression (Fig. 1C), and to ≈400% by stimulation with the phorbol ester PMA (phorbol-12-myristate-13-acetate) which activates ERK through protein kinase C (PKC) (33) (Fig. 1D). Finally, the EGF response was inhibited by double knockdown of MEK1 and MEK2 (MEK1/2) (Fig. 1E) or with MEK1/2 inhibitor U0126 (Fig. 1F). The effects of tyrphostin on luciferase expression (Fig. 1A) were specific because the drug inhibited phosphorylation of EGFR, MEK1/2, and ERK1/2 in EGF-stimulated samples but not in PMA-treated cells (Fig. 1G). Verification of EGFR knockdown, EGFR overexpression and MEK1/2 double knockdown are shown in Fig. 1H-J. Altogether, these observations indicate that the assay was sensitive and robust, with a wide dynamic range, and that it faithfully reproduced the EGF response along the MAPK signaling cascade.

Next, we investigated whether interfering with EGFR sorting into the multivesicular endosome and lysosome targeting affected the EGF signal. First, we depleted the ESCRT-0 subunit HRS, which initiates the sequence of ESCRT-I, -II, and -III recruitment. Depletion of HRS inhibits intralumenal vesicle formation (34-37), leading to the formation of "empty" multivesicular endosomes. In such a situation, EGFR is not targeted to lysosomes and is retained at the limiting membrane of endosomes, leading to prolonged half-life and phosphorylation of EGFR and its downstream kinases (20). Consistent with these notions, knockdown of HRS inhibited sorting of EGFR into multivesicular endosomes that had been enlarged by overexpression of the $Gln^{79}\rightarrow$Leu (Q79L) constitutively active mutant of the

small GTPase RAB5, as expected (37-39) (Fig. 2A). However, HRS knockdown did not result in increased or sustained EGF signaling in our assay (Fig. 2B). Similarly, depletion of the ESCRT-I subunit TSG101 (tumor susceptibility gene 101), which interacts with HRS (35, 40) and is required for intralumenal vesicle formation (10, 36, 41, 42), did not affect luciferase activity (Fig. 2B). This lack of effect did not result from an exhaustion of the response or technical shortcomings, because the signal could be increased by receptor overexpression or PMA stimulation (Fig. 1C-D). Finally, we confirmed our analysis by showing that knockdown of HRS or TSG101 did not significantly affect the transcriptional induction of *EGR1* and *FOS* mRNAs (Fig. 2C). Both are endogenous targets that are activated in the immediate early EGF response downstream of the ERK/MAPK cascade. Similarly, *EGR1* and *FOS* induction was unaffected after knockdown of the ATPase VPS4A (vacuolar protein sorting 4A) (Fig. 2C), an essential ESCRT-associated protein that catalyzes disassembly of the ESCRT-III complex (7).

After depletion of HRS or TSG101, EGFR degradation is reduced and phosphorylation of EGFR (34) and downstream kinases is prolonged (20), leading to the notion that signaling is sustained when ESCRT functions are blocked. We thus analyzed abundance of EGFR as well as phosphorylation state of EGFR and its downstream kinases over a time course that covered EGFR transcriptional response and degradation (43). As expected, EGFR abundance decreased after addition of EGF to mock-treated cells, with ≈25% remaining after 5 hours in the presence of cycloheximide (Fig. 2D; Fig. S1; Table S1). Knockdown of HRS or TSG101 (Fig. S2) delayed EGFR degradation to an extent similar to that previously observed by others (36, 44) and us (37), and concomitantly increased the phosphorylation state of EGFR and its downstream kinases, MEK1/2 and ERK1/2 (Fig. 2D; Fig. S1; Table S1). Similarly, knockdown of VPS4A inhibited EGFR degradation and increased the phosphorylation state of the receptor, MEK1/2 and ERK1/2 (Fig. 2D; Fig. S1; Table S1). Depletion of each different ESCRT subunit affected phosphorylation of EGFR, MEK and ERK in a similar manner. Hence, interfering with the ESCRT pathway increases the activation state of the receptor and downstream kinases, but does not enhance the transcriptional induction of the luciferase reporter gene, or the expression of the endogenous target genes *EGR1* and *FOS*.

The architecture of the EGF-dependent transcriptional response is not affected by depletion of ESCRT subunits or ESCRT-associated proteins

The apparent discrepancy between the activation state of EGFR and MAPK and the signaling output at the level of transcription prompted us to investigate the EGF response in more detail. To this end, we analyzed the HeLa cell transcriptome at various time points after EGF stimulation. The addition of EGF resulted in greater than 1.8-fold changes in the abundance of more than 260 mRNAs above or below that in serum-starved cells (Fig. 3A-B; Table S2). Normalization to mock-treated controls in the absence of EGF (lane m in Fig. 3B at time 0 min) and grouping according to the peak (or minimum) of transcription showed that the EGF response was well orchestrated in time, consistent with previous observations (43). The expression of immediate early genes, encoding primarily transcription factors such as FOS and EGR1 (Fig. 3B and Fig. S3), was stimulated within 30 min of EGF addition and then decreased at later time points. Factors encoded by these transcripts control subsequent steps of the response (43) and thus, cycloheximide was omitted to allow full deployment of the EGF response. At later time points, the transcription of a second and then a third wave of genes encoding for cellular effectors as well as additional feedback regulators was stimulated (Table S2 and Fig. S3) (43, 45).

We next determined the extent to which the expression of EGF-regulated transcripts was altered after depletion of HRS, TSG101, VPS4A, or the ESCRT-associated protein ALIX [ALG-2 (apoptosis-linked gene 2) interacting protein X], which inhibits formation of intralumenal vesicles (10, 46). Knockdown of all candidates was nearly complete at protein level (Fig. S2A). To evaluate the effects of ESCRT inactivation on the EGF transcriptional response, mRNA abundance for each time point under each knockdown condition were normalized to the mock-treated control without EGF (Fig. 3B). This analysis showed that the overall EGF-dependent response was not affected by any knockdown condition at any time point (Fig. 3A-B). The overall profile of transcripts with EGF-induced increases in abundance remained similar to that of controls, and no kinetic delay was observed. Principal component analysis showed that triplicates as well as time points clustered

together, and that the major source of data variability originated from EGF stimulation and not from the knockdowns (Fig. S2B).

To better reveal possible changes in gene expression resulting from the depletion of HRS or other ESCRTs, mRNA values for each each knockdown were normalized to the corresponding mock-treated controls at each time point. This representation minimizes the effects of EGF on transcription. Values were then ranked according to the magnitude of the effect and compared with the other knockdown conditions (Fig. S4A-D). This analysis revealed that, although only a small number of transcripts were decreased, HRS knockdown increased the abundance of 25 transcripts by >200%, several of which have been associated with cancer, cell proliferation, and NF-κB (nuclear factor κB) and cytokine signaling (Table S3). Knockdown of other ESCRTs resulted in less pronounced and fewer changes (Fig. S4A-D). Thus, in contrast to phosphorylation of EGFR, MEK and ERK (Fig. 2D and Fig. S1), gene expression seemed to not be uniformly affected by depletion of different ESCRT subunits although all act along the same pathway.

HRS and to some extent TSG101 depletion specifically affects NF-κB and cytokine signaling

To further substantiate our findings, we used an independent strategy to assess the quality of the microarray data. Transcripts were analyzed with NanoString, an approach that provides high sensitivity and broad dynamic range without the potential bias introduced by amplification (47, 48). We selected 100 genes that encode proteins involved in EGFR trafficking and signaling (Fig. 3C and Table S4A) as well as control genes for normalization and knockdown verification (Fig. S2A). Corresponding transcripts were measured in the same samples, which were used in the array-based analysis. In addition, we also included the knockdown of the Bro1 domain-containing putative phosphatase HD-PTP (His-domain-containing protein tyrosine phosphatase), which promotes EGFR degradation (49), in contrast to ALIX (49-52). Similar to microarray experiments, principle component analysis showed that triplicates and time points clustered together, with the major source of variability caused by EGF stimulation and not by knockdowns (Fig. S2C). Transcription profiles obtained with NanoString were similar to those observed with microarrays (Fig.

S2D). Differences in absolute transcription values likely reflect the higher dynamic range and sensitivity of the NanoString technology. A clear time dependence of the EGF-induced transcriptional program was observed and the overall organization of this response was not changed under any knockdown condition (Fig. 3C), as in the microarray analysis. Similarly, normalization to mock-treated samples at each time point after EGF addition (Fig. 3D) revealed knockdown effects, and, as observed in the microarray analysis (Fig. S4A-D), HRS depletion had a stronger effect than other knockdown conditions (Fig. 3D).

Beyond the observations that the general architecture of the response remained unaltered, interfering with ESCRT subunits clearly affected the expression of some specific genes. To investigate these changes in more detail, data were analyzed with the Ingenuity IPA software in an unbiased fashion to reveal possible pathways or networks common to ESCRT depletion. The most prominent network contained genes affected by depletion of HRS and TSG101, particularly at late time points after EGF stimulation. The computed network was enriched in genes implicated in NF-κB and cytokine signaling, consistent with the independent analysis of transcripts showing increased abundance after HRS knockdown (Table S3C-D). These include NFKB1 and 2, NFKBIA (or IκBα), TNFAIP3, BIRC3, IL6, PTGS2 (or cyclooxygenase 2), and CCL2 (Fig. S4E-F). The fact that the same pathway is affected by HRS or TSG101 depletion ruled out indirect or off-target effects. Manual analysis uncovered more genes of the same network that were transcriptionally affected (IL8, CXCL2, ZFAND5, and IRF1). Moreover, some genes regulating NF-κB signaling were only affected by HRS depletion (NFKBIE [or IκBε], REL and RELB, as well as RHEBL1). In general, the impact of HRS knockdown on the expression of those genes was more pronounced than that of TSG101 knockdown. Hence, although depletion of the ESCRT subunits has no overall influence on EGFR signaling, HRS and to some extent TSG101 depletion may specifically affect NF-κB and cytokine signaling in HeLa cells.

The global architecture of the response to high, low or pulsed EGF doses is similar

We wondered whether the apparent discrepancy in the knockdown effects on phosphorylation of EGFR and MAPK compared to downstream transcriptional activation might reflect differences in EGF stimulation. The transcriptomic analysis was carried out

without cycloheximide because the EGF response depends on protein synthesis, but the analysis of EGFR degradation had to be carried out with cycloheximide to prevent synthesis of new EGFR. Without cycloheximide, EGFR was re-synthesized at late time points (Fig. 4A) leading to possible reactivation of the cascade in the presence of EGF. To address this issue, cells were briefly stimulated with EGF and then further incubated without ligand. However, extent and kinetics of phosphorylation of EGFR and MAPK, with or without cycloheximide, were comparable to those observed after continuous stimulation (Fig. 4A-B and Fig. S5). Moreover, independent of the EGF stimulation condition, cycloheximide had a major impact on the activity status of cascade components, as anticipated (Text S1), and should thus be omitted when studying signaling responses.

Using NanoString, we then investigated the transcriptional response to the short pulse, or to continuous EGF stimulation using a low EGF dose, because EGFR trafficking may be differentially affected by the EGF dose (22, 26). To ensure an adequate comparison, fifty genes from previous experiments (Fig. 3C-D) were measured, and 40 new genes were selected from our microarray data (Fig. 3A-B) and 10 genes were used for normalization (and knockdown verification) (Text S2, and Fig. S6). To analyze the transcriptional response under these conditions, data were normalized to values from unstimulated cells and grouped according to the peak of induction (as in Fig. 3A-C). The global architecture of the response observed with high, low and pulsed EGF doses was similar (Fig. 4C). To reveal condition-specific effects, data were normalized to values obtained with the high EGF dose at each time point (Fig. 4D). Although the duration of transcription was reduced with the low EGF dose (Fig. 4D, 360 min), some transcripts were increased in abundance at early time points particularly after the pulse (Fig. 4D, 30 min), including transcripts encoding components of the immediate early and delayed early EGF response (for example, *EGR3*, *FOSB*, *NR4A* family members, *IL8* and *IL6*; see Fig. 3B for comparison). This temporal increase in the transcriptional response is likely due to delayed internalization of EGFR molecules or more efficient recycling. Moreover, the observations that the architecture of the response is essentially identical when triggered by a brief EGF pulse or by the continuous presence of the ligand, not only at the protein (Fig. 4A-B) but also at the transcriptional level (Fig. 4C-D), argues that the complete transcriptional

program is elicited within a short time after ligand binding. Presumably, the induction of immediate early genes such as activating transcription factors (Fig. S3A) and their regulators (Fig. S3B) is sufficient to determine subsequent events of the response and thus its architecture.

Interfering with EGFR endocytosis and ubiquitination upregulates the EGF-dependent transcriptional program

Endosomal sorting of EGFR molecules through ESCRT proteins did not appear to regulate the global architecture of the EGF transcriptional response nor its amplitude, although it may control NF-κB and cytokine signaling. We thus decided to investigate whether the EGF response was regulated by receptor sorting upstream of ESCRTs in more detail. To this end, we depleted cells of both clathrin heavy chain and dynamin 2 (Fig. S6A), both of which mediate EGFR internalization (17, 53). Cells were also depleted of both CBL and CBLB ubiquitin ligases (Fig. S6B). Although the relative contribution of their different targets, hence direct compared to indirect roles, is unclear, these proteins are involved in EGFR internalization (24, 54, 55) and cooperate in stimulus-dependent EGFR ubiquitination (56). The role of EGFR ubiquitination in internalization has been debated; however, the addition of ubiquitin to EGFR is essential for lysosomal targeting and degradation (7, 8).

As expected, EGFR degradation was reduced after EGF addition in cells prepared after double knockdown of clathrin heavy chain and dynamin 2 (Fig. 5A) or CBL and CBLB (Fig. 5B) compared to mock-treated controls. Similarly, each double knockdown also increased the amounts of phosphorylated EGFR, MEK1/2 and ERK1/2, and rapid dephosphorylation required protein synthesis (Fig. 5A-B), as expected (Fig. 4). The increased abundance and phosphorylation of EGFR abundance and the increased phosphorylation of downstream kinases (Fig. 5A-B) were comparable with each double knockdown, although effects were somewhat stronger in CBL- and CBLB-depleted cells (Fig. S7 and Table S1). Moreover, EGFR abundance and phosphorylation state in cells with these double knockdowns were similar in extent to those detected in cells depleted of ESCRTs (Fig. 2D and Fig. S1). Despite this similarity, luciferase activity in our reporter

assay was increased to ≈150% after depletion of clathrin heavy chain and dynamin 2 alone or together, compared to mock treatment (Fig. 5C), consistent with increased phosphorylation of MAPK (Fig. 5A) but in contrast to the situation observed after knockdown of ESCRT proteins (Fig. 2). Knockdown of CBL and CBLB also increased ELK1-driven luciferase expression to the same extent as knockdown of clathrin heavy chain and dynamin 2 (Fig. 5D). By contrast, double knockdown of ALIX and TSG101, to interfere simultaneously with intralumenal vesicle formation mediated by ESCRTs and by the ALIX-binding unconventional late endosomal lipid LBPA (lysobisphosphatidic acid) (57) did not cause any effect (Fig. 5D), despite efficient protein depletion (Fig. S6C). Interfering with ubiquitination had a stronger impact than depletion of ubiquitin-binding ESCRT subunits, perhaps because ubiquitin mediates interaction with multiple partners. We conclude that, although the effect of interfering with clathrin and dynamin 2 or with CBLs is the same at the protein level as interfering with ESCRT functions (compare Fig. 2D with Fig. 5A-B), the transcriptional response is different (compare Fig. 2B with Fig. 5C-D).

When stimulated with EGF, the receptor was efficiently internalized within 10 min into early endosomes containing EEA1 in mock-treated controls (Fig. 6A). Unbiased automated quantification with CellProfiler software showed that the bulk of endocytosed EGFR colocalized with EEA1 (Fig. S8A). Depletion of clathrin heavy chain or dynamin 2 inhibited the appearance of EGFR into EEA1-containing endosomes (Fig. 6B) to ≈30% of the control (Fig. S8A). However, the majority of endocytosed EGFR still colocalized with EEA1, as expected. Similarly, double knockdown of CBL and CBLB also reduced EGFR content in endosomes, although to a somewhat lesser extent, whereas depletion of HRS and TSG101 only had a small effect (Fig. 6C-E and quantification in Fig. S8A). Quantification of total EGFR fluorescence intensity per cell confirmed that these differences did not result from differences in EGFR abundance (Fig. S8B). Because EGFR internalization into EEA1-containing endosomes was reduced by double knockdown of clathrin heavy chain and dynamin 2 or CBL and CBLB (Fig. 6B-C and Fig. S8A), we quantified the receptor present at the plasma membrane in the absence of permeabilization. EGFR rapidly disappeared from the surface of mock-treated cells, with ≈20% remaining after 10 min (Fig.

S8C-D). Consistent with the inhibition of EGFR appearance in early endosomes, double knockdown of clathrin heavy chain and dynamin 2 significantly increased the abundance of EGFR at the plasma membrane, as did double knockdown of CBL and CBLB, albeit to a lesser extent, whereas knockdown of HRS or TSG101 did not have this effect (Fig. S8C-D). Eventually, internalized EGFR was transported to LAMP1-containing compartments within 60 min under all conditions tested, when analyzed in the presence of leupeptin to inhibit lysosomal degradation (Fig. S8E and S9), as expected (37).

These observations are consistent with the notion that receptor internalization is impaired after knockdown of clathrin heavy chain and dynamin 2 (17, 53). Our data also support the notion that in CBL- and CBLB-depleted cells, EGFR endocytosis is reduced (54). In addition, defective ubiquitination increases cell surface receptors by facilitating EGFR recycling (58, 59) — as may be the case to some, albeit lower, extent after HRS and TSG101 depletion (44).

To further investigate the EGF response after depletion of clathrin heavy chain and dynamin 2 or CBL and CBLB, we carried out a transcriptional analysis with NanoString (Fig. 7) of exactly the same genes as in the study of different EGF stimulation conditions (Fig. 4). In this analysis, we included cells prepared after double knockdown of ALIX and TSG101, which did not affect ELK1-driven luciferase in contrast to double knockdown of CBL and CBLB or clathrin heavy chain and dynamin 2 (Fig. 5C-D). We also included as positive controls cells that overexpressed EGFR approximately 2-fold over the endogenous amount (Fig. 1C and Fig. S6D), and cells treated with PMA which activates the ERK/MAPK cascade (Fig. 1D) through PKC rather than through EGFR (33).

When data were normalized to the corresponding time 0 values to illustrate the transcriptional response to EGF (Fig. 7A), it revealed that, like after ESCRT depletion (Fig. 3C), the overall architecture of transcription was comparable to the controls under all conditions tested, except PMA. Treatment with PMA not only increased transcription at 120 and 360 min but also shifted or prolonged the response in time (Fig. 7A and Text S2), because it increased luciferase activity in the signaling assay (Fig. 1D). This demonstrates

both that global changes in the architecture of the response can occur if triggered with appropriate stimuli, and that these changes can be detected with NanoString. To better reveal the possible effects of the treatments on transcription, data were normalized to the corresponding control values at each time point. This analysis confirmed that PMA generally increased and prolonged transcription (Fig. 7B), whereas double knockdown of ALIX and TSG101 affected transcription only at 30 min (Fig. 7B). In addition, this analysis revealed that double knockdown of clathrin heavy chain and dynamin 2 further increased the expression of many EGF-dependent transcripts at all time points (Fig. 7B). The effects of CBL and CBLB depletion were similar to those caused by double knockdown of clathrin heavy chain and dynamin 2, as were the effects of EGFR overexpression (Fig. 7B). Under each one of these three conditions, the expression of same EGF-dependent transcripts were increased, without global changes in the organization of the response (Fig. 7A). These three conditions clustered together in the principal component analysis (Text S2 and Fig. S6E-F) as well as upon unsupervised hierarchical clustering (Fig. S10). The ability of EGFR overexpression to mimic the changes in the EGF response caused by double knockdown of CBLand CBLB or clathrin heavy chain and dynamin 2 rules out the possibility that these changes are indirect or off-target.

Like many cultured cell lines, HeLa cells are immortalized by transformation. To determine whether our observations were more generally applicable, we analyzed the EGF transcriptional response in the immortalized but non-transformed epithelial cell line MCF10A, which is derived from human fibrocystic mammary tissue. To allow appropriate comparison between cell lines, transcripts were measured in samples prepared after knockdown of the ESCRT subunits HRS and TSG101 as well as after depletion of VPS4A. Double knockdown of clathrin heavy chain and dynamin 2, to inhibit internalization, as well as double knockdown of CBL and CBLB, to interfere with ubiquitination, were also included, as were samples from cells treated with PMA as a positive control. We selected a group of 56 genes (Fig. S11A), which include targets of the EGF response that have been identified by others (43) and by us (Fig. 3), as well as control genes for normalization and knockdown verification (Fig. S11B). The transcripts were analyzed using the NanoString technology. Similar to HeLa cells, principal component analysis showed that biological

triplicates clustered together (Text S3 and Fig. S11C), demonstrating excellent reproducibility, and that the effects of both double knockdowns (clathrin heavy chain and dynamin 2 or CBL and CBLB) and PMA stimulation (blue and orange circle in Fig. S11D, respectively) clustered away from other conditions. The magnitude of the overall response in MCF10A cells appeared somewhat diminished when compared to HeLa cells, presumably reflecting the relative abundance of some key factors, and thus effects of ESCRT knockdown were less pronounced than in HeLa cells. However, a clear time dependence of the EGF-induced transcriptional program was observed, whose overall organization was not changed under any knockdown condition. Knockdown effects were revealed after normalization to mock-treated samples at each time point of EGF addition. Unsupervised hierarchical clustering revealed the similarity of the effect of double knockdown of clathrin heavy chain and dynamin 2 or CBL and CBLB (blue branches in Fig. S11A), whereas PMA-stimulated samples at 120 and 360 min constitute a separate branch (orange) due to a more general increase and shift of gene expression. This analysis confirmed that interfering with internalization and ubiquitination, but not with ESCRT functions, stimulated the EGF transcriptional response without affecting its general architecture, essentially duplicating our findings in HeLa cells.

DISCUSSION

In *Drosophila*, *hrs* mutant larvae show expanded domains in the expression of EGFR signaling targets (34), and ESCRT mutants exhibit reduced degradation of the Notch receptor and ectopic Notch signaling (60-62), consistent with the notion that some ESCRTs act as tumor suppressors. However, it is not clear whether ESCRTs play this role in mammalian cells. TSG101 in particular was originally proposed to play a role in gene transcription as a cofactor or transcription factor (63), but its role in oncogenesis and transcriptional regulation, whether direct or indirect, is not clear (64), perhaps involving different mechanisms (65). Similarly, the role of HRS as a tumor suppressor has been questioned (66).

However, interfering with ESCRT functions clearly prolongs the half-life of EGFR and other receptors by reducing lysosome targeting. We found that this increase in EGFR abundance and phosphorylationdid not affect the EGF transcriptional response over the (short) time course corresponding to the full deployment of the EGF-dependent transcriptional program. By contrast, in ESCRT mutant animals over the long time course of embryogenesis, both distribution and amounts of EGFR and other receptors are eventually changed, thus altering transcription. We found that the acute EGF-dependent wave of transcription can be enhanced by increasing receptors at the cell surface and perhaps in recycling endosomes, by EGFR overexpression or by blocking internalization or ubiquitination. Overexpression increases the number of EGFR molecules, but also their residence time at the cell surface in the presence of EGF due to saturation of endocytic routes (67-69), enhancing the mitogenic potency of EGF (70). Indeed, increased abundance of EGFR or ERBB2 (or both), which results in internalization- and ubiquitination-deficient heterodimers (16, 69), can be found in many types of cancer (71).

Our data indicate that the complete and well-structured transcriptional program elicited by EGF is set in motion within a short time period after ligand binding to the receptor, by inducing the expression of immediate early genes that determine the subsequent architecture of the response. Our data also show that the transcriptional response is triggered primarily by a pool of receptor molecules present at the cell surface or on

recycling membranes. The replication of these findings in non-cancer derived normal diploid cells suggests that our conclusions are generally applicable. Early ESCRTs such as HRS and TSG101 have been proposed to function at a stage of endosome maturation from which recycling is possible, whereas ESCRT-II and -III function at a maturation stage after recycling (72). We speculate that ubiquitination defines the molecular checkpoint, beyond which receptor molecules are committed and no longer competent to influence the transcriptional response. In addition, our results indicate that interfering with early ESCRT functions, in particular HRS, affects NF-κB and cytokine signaling. However, our data also show that, once set in motion, the EGF transcriptional program is robust and tolerates changes in the timing of the activation states of the kinases, presumably due to the tight balance of feedback mechanisms (45).

MATERIALS AND METHODS

Reagents, antibodies, siRNAs and constructs

For cell culture, Dulbecco's Modified Eagle Medium (DMEM) - high glucose from Sigma-Aldrich (St. Louis, MO), or DMEM/F-12 - GlutaMAX from Gibco-BRL (Gaithersburg, MD) was used. Fetal calf serum (FCS) was from Brunschwig (Basel, Switzerland), and horse serum from BioConcept (Allschwil, Switzerland). L-glutamine, penicillin and streptomycin, phenol red-free DMEM (high glucose, 25 mM HEPES-buffered, without sodium pyruvate) and Opti-MEM Reduced Serum Medium, were all from Gibco-BRL. Human EGF (used at 1.5 or 100 ng/ml for stimulation), insulin (5 µg/ml final concentration), dexamethasone (1 µM final), AG1478 (or "tyrphostin", 150 nM final), PMA (phorbol 12-myristate 13-acetate, 10 ng/ml final), and cycloheximide (10 µg/ml final) were from Sigma. U0126 (10 µM final) was from Cell Signaling Technology (Danvers, MA), and luciferin (0.1 mM final) from Promega (Madison, WI). Transfection of cells with siRNAs was performed with Lipofectamine RNAiMAX (Invitrogen, San Diego, CA), and plasmid transfection was done with FuGENE HD Transfection Reagent (Roche Diagnostics, Basel, Switzerland). Mouse monoclonal antibodies were against EGFR (BD Biosciences, San Diego, CA), phospho-EGFR Tyr1173 (Upstate, Lake Placid, NY), MEK1/2 and phospho-ERK1/2 (Cell Signaling Technology), RAB5 (Reinhard Jahn, Goettingen, Germany), TSG101 (GeneTex, San Antonio, TX), and GFP (Roche). Polyclonal antibodies were raised in sheep against EGFR (BD Biosciences) and in rabbits against EEA1 (Alexis Biochemicals, Lausen, Switzerland), LAMP1 (Thermo Fisher Scientific, Lafayette, CO), phospho-MEK1/2 and ERK1/2, (Cell Signaling Technology), SNX3 (Wanjin Hong, Singapore), HRS (Harald Stenmark, Oslo, Norway), ALIX (Rémy Sadoul, Grenoble, France), DNM2 and CHC (Abcam, Cambridge, UK), as well as VPS4, CBL and CBLB (Santa Cruz Biotechnology, Santa Cruz, CA). Horseradish peroxidase-conjugated secondary antibodies were from Invitrogen or GE Healthcare (Chalfont St. Giles, UK), and fluorophore-coupled secondary antibodies from Jackson ImmunoResearch (West Grove, PA). Protein depletion was performed with ON-TARGETplus SMART pool siRNAs from Dharmacon (Thermo Fisher Scientific) (Table S5). Plasmids used were pEGFP-RAB5(Q79L) (Marino Zerial, Dresden, Germany), pEGFP-EGFR (Alexander

Sorkin, Pittsburgh, PA) and the parental vector pEGFP-N1 (Clonetech, Mountain View, CA).

Cell culture, transfection, EGF stimulation, harvest of cells, and Western blotting

Maintenance of HeLa luciferase reporter for ELK1 cells (HLR-ELK1; Stratagene, La Jolla, CA) was according to company´s instructions. MCF10A cells (ATTC, Manassas, VA) were grown in DMEM/F-12 medium supplemented with horse serum (5% v/v), antibiotics, 5 µg/ml insulin, 1 µM dexamethasone, and 10 ng/ml EGF. Transfection of siRNAs was performed using Lipofectamine RNAiMAX according to manufacturer´s instructions, and cells were grown for two days to a confluency of about 80%. Plasmid transfection with FuGENE HD Transfection Reagent was according to manufacturer´s instructions.

Before EGF stimulation, cells were starved for 16 hours in serum-free medium, and then (3 days after transfection) continuously stimulated for the indicated times with 100 ng/ml EGF. Other stimulation conditions were: (i) 5 min EGF pulse followed by washes and a chase with serum-free medium, (ii) continuous stimulation with 1.5 ng/ml ("low") EGF, or (iii) PMA treatment at a final concentration of 10 ng/ml. For EGFR degradation time courses, cycloheximide was added to a final concentration of 10 µg/ml. The cells were washed twice with PBS at 4°C, and harvested in cell lysis buffer (Cell Signaling Technology). Protein quantification was with the protein assay reagent from Bio-Rad Laboratories (Hercules, CA), as described (73). Samples were then processed for standard SDS-PAGE (74, 75) and Western blotting analysis (76, 77). Where indicated, quantification of Western blots was done with ImageJ software v1.45d. Further calculations and statistical analyses, two-way ANOVA and Bonferroni post hoc tests, were done with Microsoft Excel 2010 and GraphPad Prism v5.04 software. For RNA extraction, cells were scraped in 350 µl RLT lysis buffer (Qiagen, Valencia, CA), snap-frozen and stored at -80°C until RNA purification.

Microscopy

Cells were transfected as above, and the next day split into cover slip-containing dishes. Before stimulation (100 ng/ml continuous EGF, where indicated in the presence of 150 ng/ml leupeptin), cells were starved for 16 hours. Sample preparation for

immunofluorescence was as described (78, 79). Pictures were captured using a Leica TCS SP2 AOBS confocal microscope, equipped with a Leica 100x Plan-Apochromat oil immersion objective, or a Zeiss LSM 700 confocal microscope with a Zeiss 63x Plan-Apochromat oil immersion objective; total EGFR fluorescence was done with a Zeiss 20x Plan-Apochromat objective. Colocalization analysis was performed using the CellProfiler software v2.0, and quantification of total EGFR fluorescence with ImageJ. Further calculations and Student´s t-tests were done with Microsoft Excel 2010.

Live-cell signaling assay and quantitative real-time RT-PCR

To measure EGF-induced luciferase activity, HLR-ELK1 cells were split one day after transfection into 3.5 cm dishes in duplicates. The next day, cells were starved for 8 hours in serum-free DMEM, and then washed with phenol red-free DMEM supplemented with antibiotics. Stimulation was in the same medium in the continuous presence of 0.1 mM luciferin and 100 ng/ml EGF, at 37°C in a light-tight incubator. Bioluminescence was monitored continuously for up to 16 hours using Hamamatsu photomultiplier tube detector assemblies (80, 81). Photon counts were integrated over 10 min intervals. Data were analyzed with the LumiCycle v1.4 software (Actimetrics, Wilmette, IL) and Microsoft Excel 2010.

For quantitative real-time RT-PCR (qRT-PCR), purification of total RNA using the RNeasy Mini Kit from Qiagen was done according to manufacturer´s instructions. RNA concentrations were measured with the NanoDrop ND-1000 UV/Vis Spectrophotometer (NanoDrop Technologies, Wilmington, DE). 1 µg RNA was used for primer annealing (with QuantiTect Primer Assays for human *EGR1*, *FOS*, and *ACTB* from Qiagen). Reverse transcription (with SuperScript enzyme, Invitrogen), and PCR with QuantiTect SYBR Green PCR Kits (Qiagen), were done according to manufacturer´s instructions. Monitoring of cDNA amplification was with the iCycler from Bio-Rad, and data were analyzed with the iCycler IQ v3.1 software and Microsoft Excel 2010.

Sample preparation for microarray analysis

HLR-ELK1 cells were grown, transfected, starved for 16 hours, stimulated, and harvested in RLT buffer as described above. For each transfection, four time points of EGF

stimulation (0, 30, 120, and 360 min) were assayed in independent biological triplicates, and one dish was prepared simultaneously to determine protein depletion by Western blotting. The same lots and batches of media, FCS, transfection reagents, siRNAs, and EGF or PMA were used throughout the procedure, to exclude any possible batch effects. Purification of total RNA was as above. Concentration, purity and integrity of the RNA were measured with the Picodrop Microliter UV/Vis Spectrophotometer (Picodrop, Saffron Walden, UK), and the Agilent 2100 Bioanalyzer (Agilent Technologies, Santa Clara, CA), together with the RNA 6000 Series II Nano Kit (Agilent) according to manufacturer´s instructions.

We used the Human Gene 1.0 ST Array Reagent Kit (Affymetrix, High Wycombe, Buckinghamshire, UK) for microarray target amplification, and for labeling we used the GeneChip Whole Transcript Sense Target Labeling Assay (Affymetrix). Target preparation as well as hybridization, washing and scanning was performed according to manufacturer´s instructions, as described (82). In general, all samples were processed simultaneously, except for cleanup steps and the hybridization till scanning procedure. There, one replicate of each condition was processed at the same time, in order to minimize possible batch effects due to sample handling. Sample preparation was according to the 100 ng Total RNA Labeling Protocol. Differing from the protocol, 200 ng of total RNA were used as starting material for the first-strand cDNA synthesis.

mRNA measurements using the NanoString technology

The same samples analyzed by microarrays were also measured with the NanoString nCounter gene expression system (47, 48) from NanoString Technologies (Seattle, WA). A second, independent measurement was performed in HeLa (HLR-ELK1) cells, and a third experiment was done with MCF10A cells. All target sequences for the three NanoString analyses are summarized in Table S4A-C. Cell growth, transfection, starvation, stimulation, and harvest were identical to the microarray experiment, except that DMEM/F-12 medium was used for MCF10A cells, and biological triplicates were prepared for each condition. Assay set-up (combining reporter probes, mRNA, and capture probes), hybridization at 65°C for at least 12 hours, post-hybridization processing using the nCounter Prep Station, and scanning with the nCounter Digital Analyzer (NanoString) were done according to

manufacturer´s instructions, as described (83), except that 300 ng of mRNA were used as starting material.

Software used for normalization and analysis of transcriptome data

The raw microarray data files were generated using the Affymetrix GeneChip Operating Software. Normalization (according to the RMA procedure) was done with Partek Genomics Suite v6.5 (St. Louis, MO), and a batch removal step was performed to eliminate possible effects of the scan date. We used R.2.6 together with the affy, limma and geneplotter packages from the bioconductor platform and MS Excel 2010 in order to: (i) further normalize (to the mock-treated sample at time 0 to illustrate the EGF response, or to the corresponding mock values at each time point to visualize effects of the various conditions); (ii) define a cut-off (1.8-fold difference to mock 0 min EGF); (iii) group (according to the peak of expression); and (iv) rank genes (according to the strength of induction). Values from NanoString measurements were normalized to multiple housekeeping genes (84), using an Excel-based macro (83). Further normalization, grouping and ranking was as above.

Heat maps were created with Partek, and additionally processed for visualization with Adobe Illustrator CS4 v14.0 (Adobe, San Jose, CA). GeneSpring GX v7.3 (Agilent) and MS Excel was used to create lists of affected genes in knockdown conditions, and pathway analysis was performed for those genes with Ingenuity pathway analysis IPA v7.6 software (Ingenuity Systems, Redwood City, CA). Lists of EGF-induced genes and of genes affected by knockdowns in the microarray analysis can be found in Table S2 and S3A-D, respectively (85).

SUPPLEMENTARY MATERIALS

Text S1. Analysis of the different conditions of stimulation.

Text S2. Quality control for the second NanoString analysis.

Text S3. Quality control for the third NanoString analysis.

Fig. S1. Quantification of EGFR, as well as phosphorylated EGFR and downstream kinases, after depletion of ESCRT proteins.

Fig. S2. Quality controls for microarrays and the first NanoString measurement.

Fig. S3. Known EGF-induced feedback regulators from microarray analysis.

Fig. S4. Magnitude and comparison of ESCRT knockdown effects in the microarrays, and network analysis of HRS and TSG101 knockdown effects.

Fig. S5. Quantification of EGFR, as well as phosphorylated EGFR and downstream kinases, under different conditions of stimulation with EGF.

Fig. S6. Quality controls for the second NanoString experiment and comparison to the first data set.

Fig. S7. Quantification of abundance and phosphorylation of EGFR and phosphorylation of downstream kinases after various double knockdowns.

Fig. S8. Analysis of EGFR distribution.

Fig. S9. EGFR localization after 60 min of EGF stimulation.

Fig. S10. Hierarchical clustering of the transcriptional response and of effects in the second NanoString experiment.

Fig. S11. Hierarchical clustering of effects in the third NanoString experiment and quality controls.

Table S1. Two-way ANOVA analysis of quantification of EGFR and phosphorylated EGFR, MEK1/2, or ERK1/2.

Table S2. Microarray analysis of EGF response genes.

Table S3. Microarray analysis of knockdown effects.

Table S4. Target sequences of the NanoString code sets.

Table S5. siRNA target sequences.

Table S6. Microarray analysis of all EGF response genes.

REFERENCES AND NOTES

1. Carpenter, G., and S. Cohen. 1979. Epidermal growth factor. *Annu Rev Biochem* 48: 193-216.
2. Dunn, W. A., T. P. Conolly, and A. Hubbard. 1986. Receptor-mediated endocytosis of epidermal growth factor by rat hepatocytes: receptor pathway. *J. Cell Biol.* 102: 24-36.
3. Miller, K., J. Beardmore, H. Kanety, J. Schlessinger, and C. R. Hopkins. 1986. Localization of the epidermal growth factor (EGF) receptor within the endosome of EGF-stimulated epidermoid carcinoma (A431) cells. *J Cell Biol* 102: 500-509.
4. Lai, W. H., H. J. Guyda, and J. J. Bergeron. 1986. Binding and internalization of epidermal growth factor in human term placental cells in culture. *Endocrinology* 118: 413-423.
5. Woodman, P. G., and C. E. Futter. 2008. Multivesicular bodies: co-ordinated progression to maturity. *Curr Opin Cell Biol* 20: 408-414.
6. Piper, R. C., and D. J. Katzmann. 2007. Biogenesis and Function of Multivesicular Bodies. *Annu Rev Cell Dev Biol*.
7. Hurley, J. H., and P. I. Hanson. 2010. Membrane budding and scission by the ESCRT machinery: it's all in the neck. *Nat Rev Mol Cell Biol* 11: 556-566.
8. Raiborg, C., and H. Stenmark. 2009. The ESCRT machinery in endosomal sorting of ubiquitylated membrane proteins. *Nature* 458: 445-452.
9. Saksena, S., J. Wahlman, D. Teis, A. E. Johnson, and S. D. Emr. 2009. Functional reconstitution of ESCRT-III assembly and disassembly. *Cell* 136: 97-109.
10. Falguières, T., P. P. Luyet, C. Bissig, C. C. Scott, M.-C. Velluz, and J. Gruenberg. 2008. In vitro budding of intralumenal vesicles into late endosomes is regulated by Alix and Tsg101. *Mol Biol Cell* 19: 4942-4955.
11. White, I. J., L. M. Bailey, M. R. Aghakhani, S. E. Moss, and C. E. Futter. 2006. EGF stimulates annexin 1-dependent inward vesiculation in a multivesicular endosome subpopulation. *Embo J* 25: 1-12.
12. Stuffers, S., C. Sem Wegner, H. Stenmark, and A. Brech. 2009. Multivesicular endosome biogenesis in the absence of ESCRTs. *Traffic* 10: 925-937.
13. Baass, P. C., G. M. Di Guglielmo, F. Authier, B. I. Posner, and J. J. Bergeron. 1995. Compartmentalized signal transduction by receptor tyrosine kinases. *Trends Cell Biol* 5: 465-470.
14. Miaczynska, M., L. Pelkmans, and M. Zerial. 2004. Not just a sink: endosomes in control of signal transduction. *Curr Opin Cell Biol* 16: 400-406.
15. Zweifel, L. S., R. Kuruvilla, and D. D. Ginty. 2005. Functions and mechanisms of retrograde neurotrophin signalling. *Nat Rev Neurosci* 6: 615-625.
16. Citri, A., and Y. Yarden. 2006. EGF-ERBB signalling: towards the systems level. *Nat Rev Mol Cell Biol* 7: 505-516.
17. Sorkin, A., and M. von Zastrow. 2009. Endocytosis and signalling: intertwining molecular networks. *Nat Rev Mol Cell Biol* 10: 609-622.
18. Polo, S., and P. P. Di Fiore. 2006. Endocytosis conducts the cell signaling orchestra. *Cell* 124: 897-900.

19. Kholodenko, B. N., J. F. Hancock, and W. Kolch. 2010. Signalling ballet in space and time. *Nat Rev Mol Cell Biol* 11: 414-426.
20. Wegner, C. S., L. M. Rodahl, and H. Stenmark. 2011. ESCRT Proteins and Cell Signalling. *Traffic*.
21. Vieira, A. V., C. Lamaze, and S. L. Schmid. 1996. Control of EGF receptor signaling by clathrin-mediated endocytosis. *Science* 274: 2086-2089.
22. Sigismund, S., E. Argenzio, D. Tosoni, E. Cavallaro, S. Polo, and P. P. Di Fiore. 2008. Clathrin-mediated internalization is essential for sustained EGFR signaling but dispensable for degradation. *Dev Cell* 15: 209-219.
23. Chen, H., and P. De Camilli. 2005. The association of epsin with ubiquitinated cargo along the endocytic pathway is negatively regulated by its interaction with clathrin. *Proc Natl Acad Sci U S A* 102: 2766-2771.
24. Sigismund, S., T. Woelk, C. Puri, E. Maspero, C. Tacchetti, P. Transidico, P. P. Di Fiore, and S. Polo. 2005. Clathrin-independent endocytosis of ubiquitinated cargos. *Proc Natl Acad Sci U S A* 102: 2760-2765.
25. Madshus, I. H., and E. Stang. 2009. Internalization and intracellular sorting of the EGF receptor: a model for understanding the mechanisms of receptor trafficking. *J Cell Sci* 122: 3433-3439.
26. Sorkin, A., S. Krolenko, N. Kudrjavtceva, J. Lazebnik, L. Teslenko, A. M. Soderquist, and N. Nikolsky. 1991. Recycling of epidermal growth factor-receptor complexes in A431 cells: identification of dual pathways. *J Cell Biol* 112: 55-63.
27. Di Guglielmo, G. M., P. C. Baass, W. J. Ou, B. I. Posner, and J. J. Bergeron. 1994. Compartmentalization of SHC, GRB2 and mSOS, and hyperphosphorylation of Raf-1 by EGF but not insulin in liver parenchyma. *EMBO J* 13: 4269-4277.
28. Gonzalez-Gaitan, M., and H. Stenmark. 2003. Endocytosis and signaling: a relationship under development. *Cell* 115: 513-521.
29. Teis, D., W. Wunderlich, and L. A. Huber. 2002. Localization of the MP1-MAPK scaffold complex to endosomes is mediated by p14 and required for signal transduction. *Dev Cell* 3: 803-814.
30. Nada, S., A. Hondo, A. Kasai, M. Koike, K. Saito, Y. Uchiyama, and M. Okada. 2009. The novel lipid raft adaptor p18 controls endosome dynamics by anchoring the MEK-ERK pathway to late endosomes. *Embo J* 28: 477-489.
31. Kelemen, B. R., K. Hsiao, and S. A. Goueli. 2002. Selective in vivo inhibition of mitogen-activated protein kinase activation using cell-permeable peptides. *The Journal of biological chemistry* 277: 8741-8748.
32. Yaish, P., A. Gazit, C. Gilon, and A. Levitzki. 1988. Blocking of EGF-dependent cell proliferation by EGF receptor kinase inhibitors. *Science* 242: 933-935.
33. Seger, R., and E. G. Krebs. 1995. The MAPK signaling cascade. *FASEB J* 9: 726-735.
34. Lloyd, T. E., R. Atkinson, M. N. Wu, Y. Zhou, G. Pennetta, and H. J. Bellen. 2002. Hrs regulates endosome membrane invagination and tyrosine kinase receptor signaling in Drosophila. *Cell* 108: 261-269.
35. Bache, K. G., A. Brech, A. Mehlum, and H. Stenmark. 2003. Hrs regulates multivesicular body formation via ESCRT recruitment to endosomes. *J Cell Biol* 162: 435-442.
36. Razi, M., and C. E. Futter. 2006. Distinct roles for Tsg101 and Hrs in multivesicular body formation and inward vesiculation. *Mol Biol Cell* 17: 3469-3483.

37. Pons, V., P. P. Luyet, E. Morel, L. Abrami, F. G. van der Goot, R. G. Parton, and J. Gruenberg. 2008. Hrs and SNX3 functions in sorting and membrane invagination within multivesicular bodies. *PLoS Biol* 6: e214.
38. Raiborg, C., K. G. Bache, D. J. Gillooly, I. H. Madshus, E. Stang, and H. Stenmark. 2002. Hrs sorts ubiquitinated proteins into clathrin-coated microdomains of early endosomes. *Nat Cell Biol* 4: 394-398.
39. Trajkovic, K., C. Hsu, S. Chiantia, L. Rajendran, D. Wenzel, F. Wieland, P. Schwille, B. Brugger, and M. Simons. 2008. Ceramide triggers budding of exosome vesicles into multivesicular endosomes. *Science* 319: 1244-1247.
40. Pornillos, O., D. S. Higginson, K. M. Stray, R. D. Fisher, J. E. Garrus, M. Payne, G. P. He, H. E. Wang, S. G. Morham, and W. I. Sundquist. 2003. HIV Gag mimics the Tsg101-recruiting activity of the human Hrs protein. *J Cell Biol* 162: 425-434.
41. Doyotte, A., M. R. Russell, C. R. Hopkins, and P. G. Woodman. 2005. Depletion of TSG101 forms a mammalian "Class E" compartment: a multicisternal early endosome with multiple sorting defects. *J Cell Sci* 118: 3003-3017.
42. Wollert, T., and J. H. Hurley. 2010. Molecular mechanism of multivesicular body biogenesis by ESCRT complexes. *Nature*.
43. Amit, I., A. Citri, T. Shay, Y. Lu, M. Katz, F. Zhang, G. Tarcic, D. Siwak, J. Lahad, J. Jacob-Hirsch, N. Amariglio, N. Vaisman, E. Segal, G. Rechavi, U. Alon, G. B. Mills, E. Domany, and Y. Yarden. 2007. A module of negative feedback regulators defines growth factor signaling. *Nat Genet* 39: 503-512.
44. Raiborg, C., L. Malerod, N. M. Pedersen, and H. Stenmark. 2008. Differential functions of Hrs and ESCRT proteins in endocytic membrane trafficking. *Exp Cell Res* 314: 801-813.
45. Avraham, R., and Y. Yarden. 2011. Feedback regulation of EGFR signalling: decision making by early and delayed loops. *Nature reviews. Molecular cell biology* 12: 104-117.
46. Matsuo, H., J. Chevallier, N. Mayran, I. Le Blanc, C. Ferguson, J. Fauré, N. Sartori-Blanc, S. Matile, J. Dubochet, R. Sadoul, R. G. Parton, F. Vilbois, and J. Gruenberg. 2004. Role of LBPA and Alix in multivesicular liposome formation and endosome organization. *Science* 303: 531-534.
47. Geiss, G. K., R. E. Bumgarner, B. Birditt, T. Dahl, N. Dowidar, D. L. Dunaway, H. P. Fell, S. Ferree, R. D. George, T. Grogan, J. J. James, M. Maysuria, J. D. Mitton, P. Oliveri, J. L. Osborn, T. Peng, A. L. Ratcliffe, P. J. Webster, E. H. Davidson, L. Hood, and K. Dimitrov. 2008. Direct multiplexed measurement of gene expression with color-coded probe pairs. *Nat Biotechnol* 26: 317-325.
48. Malkov, V. A., K. A. Serikawa, N. Balantac, J. Watters, G. Geiss, A. Mashadi-Hossein, and T. Fare. 2009. Multiplexed measurements of gene signatures in different analytes using the Nanostring nCounter Assay System. *BMC Res Notes* 2: 80.
49. Doyotte, A., A. Mironov, E. McKenzie, and P. Woodman. 2008. The Bro1-related protein HD-PTP/PTPN23 is required for endosomal cargo sorting and multivesicular body morphogenesis. *Proc Natl Acad Sci U S A* 105: 6308-6313.
50. Luyet, P. P., T. Falguieres, V. Pons, A. K. Pattnaik, and J. Gruenberg. 2008. The ESCRT-I subunit TSG101 controls endosome-to-cytosol release of viral RNA. *Traffic* 9: 2279-2290.

51. Cabezas, A., K. G. Bache, A. Brech, and H. Stenmark. 2005. Alix regulates cortical actin and the spatial distribution of endosomes. *J Cell Sci* 118: 2625-2635.
52. Schmidt, M. H., D. Hoeller, J. Yu, F. B. Furnari, W. K. Cavenee, I. Dikic, and O. Bogler. 2004. Alix/AIP1 antagonizes epidermal growth factor receptor downregulation by the Cbl-SETA/CIN85 complex. *Mol Cell Biol* 24: 8981-8993.
53. Zwang, Y., and Y. Yarden. 2009. Systems biology of growth factor-induced receptor endocytosis. *Traffic* 10: 349-363.
54. Huang, F., L. K. Goh, and A. Sorkin. 2007. EGF receptor ubiquitination is not necessary for its internalization. *Proc Natl Acad Sci U S A* 104: 16904-16909.
55. Dikic, I., S. Wakatsuki, and K. J. Walters. 2009. Ubiquitin-binding domains - from structures to functions. *Nature reviews. Molecular cell biology* 10: 659-671.
56. Pennock, S., and Z. Wang. 2008. A tale of two Cbls: interplay of c-Cbl and Cbl-b in epidermal growth factor receptor downregulation. *Mol Cell Biol* 28: 3020-3037.
57. Falguieres, T., P. P. Luyet, and J. Gruenberg. 2009. Molecular assemblies and membrane domains in multivesicular endosome dynamics. *Exp Cell Res* 315: 1567-1573.
58. Grovdal, L. M., E. Stang, A. Sorkin, and I. H. Madshus. 2004. Direct interaction of Cbl with pTyr 1045 of the EGF receptor (EGFR) is required to sort the EGFR to lysosomes for degradation. *Exp Cell Res* 300: 388-395.
59. McCullough, J., M. J. Clague, and S. Urbe. 2004. AMSH is an endosome-associated ubiquitin isopeptidase. *J Cell Biol* 166: 487-492.
60. Moberg, K. H., S. Schelble, S. K. Burdick, and I. K. Hariharan. 2005. Mutations in erupted, the Drosophila ortholog of mammalian tumor susceptibility gene 101, elicit non-cell-autonomous overgrowth. *Dev Cell* 9: 699-710.
61. Thompson, B. J., J. Mathieu, H. H. Sung, E. Loeser, P. Rorth, and S. M. Cohen. 2005. Tumor suppressor properties of the ESCRT-II complex component Vps25 in Drosophila. *Dev Cell* 9: 711-720.
62. Vaccari, T., and D. Bilder. 2005. The Drosophila tumor suppressor vps25 prevents nonautonomous overproliferation by regulating notch trafficking. *Dev Cell* 9: 687-698.
63. Li, L., and S. N. Cohen. 1996. Tsg101: a novel tumor susceptibility gene isolated by controlled homozygous functional knockout of allelic loci in mammalian cells. *Cell* 85: 319-329.
64. Tanaka, N., M. Kyuuma, and K. Sugamura. 2008. Endosomal sorting complex required for transport proteins in cancer pathogenesis, vesicular transport, and non-endosomal functions. *Cancer science* 99: 1293-1303.
65. Roxrud, I., H. Stenmark, and L. Malerod. 2010. ESCRT & Co. *Biol Cell* 102: 293-318.
66. Toyoshima, M., N. Tanaka, J. Aoki, Y. Tanaka, K. Murata, M. Kyuuma, H. Kobayashi, N. Ishii, N. Yaegashi, and K. Sugamura. 2007. Inhibition of tumor growth and metastasis by depletion of vesicular sorting protein Hrs: its regulatory role on E-cadherin and beta-catenin. *Cancer research* 67: 5162-5171.
67. Wiley, H. S. 1988. Anomalous binding of epidermal growth factor to A431 cells is due to the effect of high receptor densities and a saturable endocytic system. *J Cell Biol* 107: 801-810.

68. Lund, K. A., L. K. Opresko, C. Starbuck, B. J. Walsh, and H. S. Wiley. 1990. Quantitative analysis of the endocytic system involved in hormone-induced receptor internalization. *J Biol Chem* 265: 15713-15723.
69. Sorkin, A., and L. K. Goh. 2009. Endocytosis and intracellular trafficking of ErbBs. *Exp Cell Res* 315: 683-696.
70. Traverse, S., K. Seedorf, H. Paterson, C. J. Marshall, P. Cohen, and A. Ullrich. 1994. EGF triggers neuronal differentiation of PC12 cells that overexpress the EGF receptor. *Curr Biol* 4: 694-701.
71. Hynes, N. E., and G. MacDonald. 2009. ErbB receptors and signaling pathways in cancer. *Current opinion in cell biology* 21: 177-184.
72. Rodahl, L. M., S. Stuffers, V. H. Lobert, and H. Stenmark. 2009. The role of ESCRT proteins in attenuation of cell signalling. *Biochem Soc Trans* 37: 137-142.
73. Bradford, M. M. 1976. A rapid and sensitive method for the quantitation of microgram quantities of protein utilizing the principle of protein-dye binding. *Anal Biochem* 72: 248-254.
74. Shapiro, A. L., E. Vinuela, and J. V. Maizel, Jr. 1967. Molecular weight estimation of polypeptide chains by electrophoresis in SDS-polyacrylamide gels. *Biochem Biophys Res Commun* 28: 815-820.
75. Laemmli, U. K. 1970. Cleavage of structural proteins during the assembly of the head of bacteriophage T4. *Nature* 227: 680-685.
76. Towbin, H., T. Staehelin, and J. Gordon. 1979. Electrophoretic transfer of proteins from polyacrylamide gels to nitrocellulose sheets: procedure and some applications. *Proc Natl Acad Sci U S A* 76: 4350-4354.
77. Burnette, W. N. 1981. "Western blotting": electrophoretic transfer of proteins from sodium dodecyl sulfate--polyacrylamide gels to unmodified nitrocellulose and radiographic detection with antibody and radioiodinated protein A. *Anal Biochem* 112: 195-203.
78. Gu, F., F. Aniento, R. G. Parton, and J. Gruenberg. 1997. Functional dissection of COP-I subunits in the biogenesis of multivesicular endosomes. *J Cell Biol* 139: 1183-1195.
79. Kobayashi, T., E. Stang, K. S. Fang, P. de Moerloose, R. G. Parton, and J. Gruenberg. 1998. A lipid associated with the antiphospholipid syndrome regulates endosome structure and function. *Nature* 392: 193-197.
80. Yamazaki, S., R. Numano, M. Abe, A. Hida, R. Takahashi, M. Ueda, G. D. Block, Y. Sakaki, M. Menaker, and H. Tei. 2000. Resetting central and peripheral circadian oscillators in transgenic rats. *Science* 288: 682-685.
81. Yoo, S. H., S. Yamazaki, P. L. Lowrey, K. Shimomura, C. H. Ko, E. D. Buhr, S. M. Siepka, H. K. Hong, W. J. Oh, O. J. Yoo, M. Menaker, and J. S. Takahashi. 2004. PERIOD2::LUCIFERASE real-time reporting of circadian dynamics reveals persistent circadian oscillations in mouse peripheral tissues. *Proc Natl Acad Sci U S A* 101: 5339-5346.
82. Rossner, M. J., J. Hirrlinger, S. P. Wichert, C. Boehm, D. Newrzella, H. Hiemisch, G. Eisenhardt, C. Stuenkel, O. von Ahsen, and K. A. Nave. 2006. Global transcriptome analysis of genetically identified neurons in the adult cortex. *The Journal of neuroscience : the official journal of the Society for Neuroscience* 26: 9956-9966.

83. Beaume, M., D. Hernandez, M. Docquier, C. Delucinge-Vivier, P. Descombes, and P. Francois. 2011. Orientation and expression of methicillin-resistant Staphylococcus aureus small RNAs by direct multiplexed measurements using the nCounter of NanoString technology. *Journal of microbiological methods* 84: 327-334.

84. Vandesompele, J., K. De Preter, F. Pattyn, B. Poppe, N. Van Roy, A. De Paepe, and F. Speleman. 2002. Accurate normalization of real-time quantitative RT-PCR data by geometric averaging of multiple internal control genes. *Genome Biol* 3: RESEARCH0034.

85. **Acknowledgements:** We are grateful to Marie-Claire Velluz for technical assistance. We are very grateful to Patrick Descombes and Mylène Docquier from the Geneva Genomics platform for help with the NanoString experiments and Christoph Bauer from the Geneva Bioimaging platform. We are also grateful to Cameron Scott and Fabrizio Vacca for critically reading the manuscript. **Funding:** Support to JG was from the Swiss National Science Foundation, the Telethon Foundation, PRISM from the EU Sixth Framework Program, the NCCR in Chemical Biology and LipidX from the Swiss SystemsX.ch initiative, evaluated by the Swiss National Science Foundation. MJR and SPW acknowledge support by the German Bundesministerium für Bildung und Forschung (BMBF grant VIP-16V0008). **Author contributions:** BB conceived, designed and performed all experiments, and wrote the manuscript**.** SPW performed the microarray experiments, and helped with data analysis. SDJ helped with microscopy and quantified immunofluorescence pictures. OS helped with microarray and NanoString analyses. MJR helped with the microarray experiments and data analysis. JG conceived and designed the experiments and wrote the manuscript. **Competing interests:** The authors declare that they have no competing interests.

FIGURE LEGENDS

Fig. 1. Live-cell signaling assay. (**A**) Luciferase activity was measured while incubating HLR-ELK1 cells without (grey) or with 100 ng/ml EGF alone (black) or with AG1478 (red). The raw data (in separate duplicates) are normalized to protein. (**B**) Luciferase activity in mock-treated (black) or EGFR-depleted (red) cells was normalized as time "0" to the mock peak value (n = 2 experiments, each in duplicates). (**C-F**) Luciferase activity was measured and normalized as in (B) in cells expressing GFP (black) or GFP-EGFR (red; n = 4 experiments) (C), cells treated with EGF (black) or PMA (red; n = 7 experiments) (D), mock-treated (black) or treated with siRNAs against MEK1 and MEK2 (red; n = 2 experiments) (E), treated with EGF in the absence (black) or presence (red) of U0126 (n = 2 experiments) (F). (**G**) Cells were treated with EGF or PMA with or without AG1478 and analyzed by Western blotting using antibodies against EGFR or the phosphorylated forms (P-) of the indicated proteins. (**H-J**) Cells treated with siRNAs against EGFR (H) or MEK1 and MEK2 (J) or cells overexpressing GFP-EGFR (I) were analyzed by Western blotting.

Fig. 2. Receptor sorting, signaling and phosphorylation after depletion of ESCRT proteins. (**A**) Cells treated (KD) or not (mock) with HRS siRNAs and expressing GFP-RAB5(Q79L) were incubated with EGF for 30 min and analyzed by indirect immunofluorescence with anti-EGFR antibody. In the right panel, EGFR in the endosome lumen is expressed as a percentage of the total in each endosome (≥ 30 endosome scans per condition; ****P < 0.0001, Student´s t-test; n = 4 experiments). Scale bar, 10 μm. (**B**) Luciferase activity in mock-treated (black) or in cells treated with siRNAs against HRS (green) or TSG101 (blue) was measured and normalized as in Fig. 1B-F (TSG101, n = 10 experiments; HRS, n = 5 experiments). (**C**) Cells mock-treated or treated with siRNAs against the indicated targets were incubated with EGF for 0 or 30 min and then analyzed by qRT-PCR for endogenous *EGR1* and *FOS* mRNAs. Data represent ddCt values (number of PCR cycles between non-induced and EGF-induced, normalized to actin) (P > 0.05, Student´s t-test; n = 3 experiments performed in triplicates). (**D**) Cells mock-treated or treated with siRNAs

against the indicated targets were stimulated with EGF in the presence of cycloheximide for the indicated time (in hours), and analyzed by Western blotting as in Fig. 1G (quantification in Fig. S1 and statistical analysis in Table S1).

Fig. 3. Architecture of the transcriptional EGF response after ESCRT depletion. (**A-B**) Cells mock-treated (m) or treated with siRNAs against HRS (H), TSG101 (T), VPS4A (V) or ALIX (A), were incubated with EGF for the indicated time. The heat map in (A) shows 263 genes whose transcription was at least 1.8-fold above or below that in mock-treated samples at t = 0 min (no EGF). Data represent means of independent biological triplicates, and values for each gene are normalized to mock-treated controls at t = 0 min (white; fold change = 1; log2(1) = 0). Genes were further grouped according to their peak (or minimum) of expression in mock-treated cells and ranked according to decreasing fold change. (B) shows a magnified view of immediate early and top delayed early genes from (A). (**C** and **D**) 100 genes (Table S4A) from the same samples as in (A) and (B) were analyzed using NanoString, including HD-PTP (P) knockdown samples prepared in parallel. In (C), normalization, grouping and ranking was as in (A). In (D), values were normalized to the mock-treated controls at each time point. White lanes (fold change = 0) corresponding to mock-treated controls were omitted for clarity. All values are given as log2.

Fig. 4. Effect of different EGF stimulation conditions on the transcriptional response. (**A**) Cells treated with 100 ng/ml EGF for the indicated time (in hours), with or without cycloheximide, were analyzed by Western blotting as in Fig. 2D. (**B**) As in (A), except that cells were treated with EGF for 5 min only followed by washes and a chase without EGF in serum-free medium. Quantification of the data in (A) and (B) is in Fig. S5 and statistical analysis in Table S1. (**C** and **D**) Cells were incubated for the indicated time in the absence of cycloheximide without or with 100 ng/ml EGF (high) as in (A), or with 1.5 ng/ml (low). Alternatively, cells were treated with 100 ng/ml EGF for 5 min in the absence of cycloheximide followed by a chase (p-ch) as in (B). The same group of 100 transcripts as in Fig. 7 was analyzed by NanoString (Table S4B; for quality controls see Text S2 and Fig. S6). In (C), data are normalized to values of unstimulated control samples, grouped and

ranked as in Fig. 3A-C. The t = 0 min control lane (white, fold change = 0) was omitted for clarity. In (D), the different stimulation conditions are compared by normalizing data to the corresponding values obtained after continuous stimulation with 100 ng/ml EGF. Values in (C) and (D) are in log2.

Fig. 5. Interfering with internalization and ubiquitination. (**A**) Cells mock-treated or treated with siRNAs against both clathrin heavy chain and dynamin 2 (C + D2) were incubated with EGF for the indicated time (hours) in the presence or absence of cycloheximide. Samples were analyzed by Western blotting with antibodies that recognize EGFR, RAB5 or the phosphorylated forms of EGFR and downstream kinases. (**B**) Cells mock-treated or treated with siRNAs against both CBL and CBLB (B + C-CBL) were analyzed as in (A). Quantification of the data in (A) and (B) is in Fig. S7 and statistical analysis is in Table S1. (**C**) Luciferase activity was measured as in Fig. 1 and 2B in mock-treated (black) or in cells treated with siRNAs against clathrin heavy chain (dark red; n = 7 experiments), dynamin 2 (red; n = 7 experiments), or both as in (A) (orange; n = 3 experiments). (**D**) Luciferase activity was measured in mock-treated (black) or in cells treated with siRNAs against CBL and CBLB as in (B) (green; n = 6 experiments) or against ALIX and TSG101 (blue; n = 3 experiments). Data in (C) and (D) are normalized to the peak value of control cells.

Fig. 6. EGFR distribution after 10 min of EGF stimulation. (**A** to **E**) Cells were mock-treated (A) or treated with siRNAs against both clathrin heavy chain and dynamin 2 (B), CBL and CBLB (C), HRS (D), or TSG101 (E), and then incubated with EGF. Cells were analyzed by indirect immunofluorescence using antibodies against EGFR and EEA1. Quantification of the data is shown in Fig. S8A, quantification of total EGFR fluorescence is in Fig. S8B, and surface EGFR staining and quantification under the different knockdown conditions is in Fig. S8C-D. EGFR distribution after 60 min is shown in Fig. S9. Scale bar is 10 μm.

Fig. 7. Comparative analysis of the transcriptional response. (**A**) Cells were mock-treated (Ctr) or treated with siRNAs against both clathrin heavy chain and dynamin 2 (C + D2),

against both CBLB and CBL (B + C), or against both ALIX and TSG101 (A + T) and then incubated with EGF for the indicated time. Cells overexpressing the EGFR were challenged with EGF, or cells were treated with PMA. A selected group of 100 transcripts (corresponding to Fig. 4) was analyzed by NanoString (see Table S4B and quality controls in Fig. S6). Data are normalized to values in unstimulated samples, grouped and ranked as in Fig. 3A-C and Fig. 4C. The t = 0 min control lanes (white, fold change = 0) were omitted for clarity. (**B**) The different treatments in (A) are compared to the values obtained with the EGF-treated controls. Data are normalized to each control at the corresponding time points. All values are in log2.

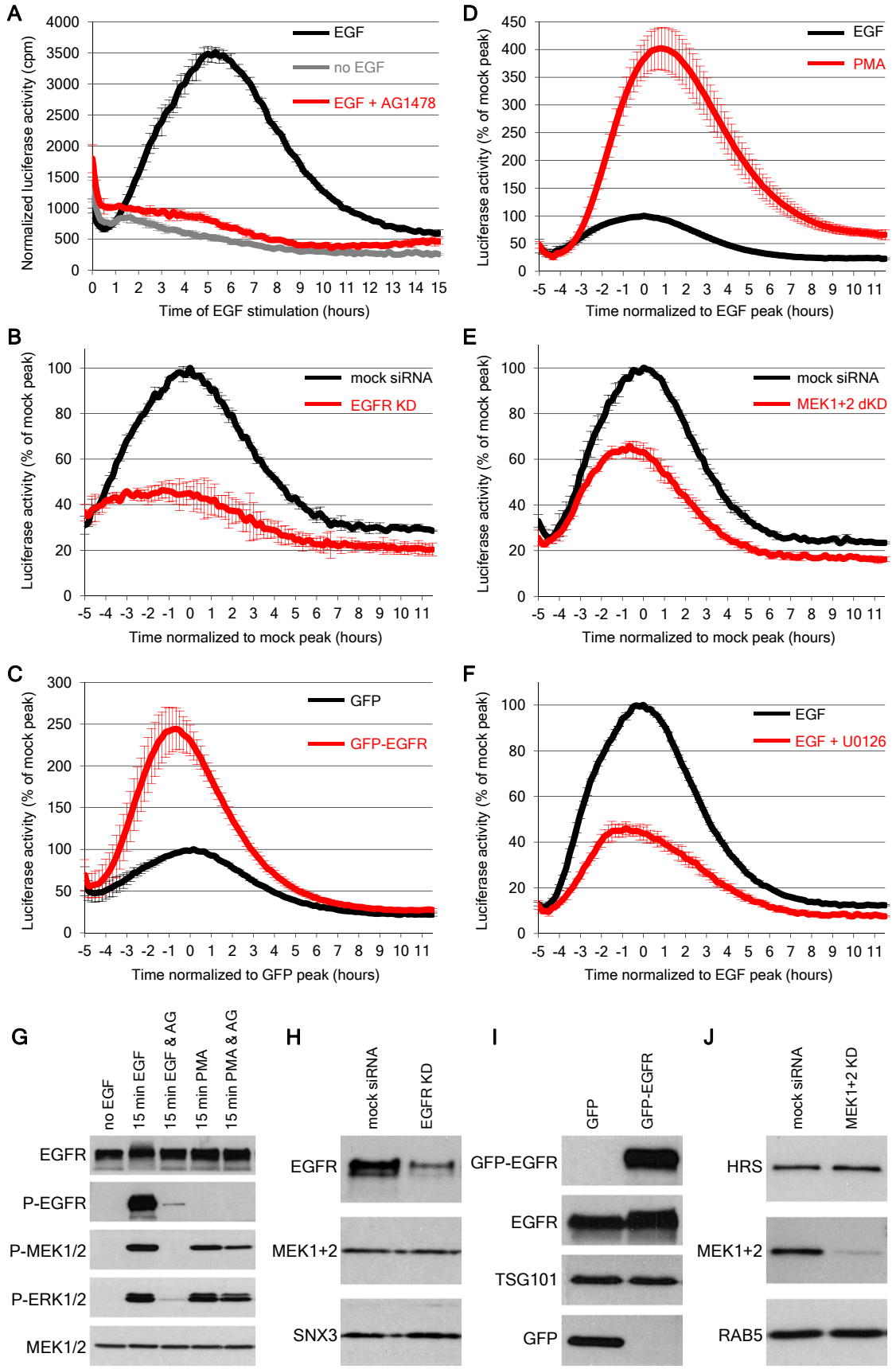
A
Normalized luciferase activity (cpm)
Time of EGF stimulation (hours)
EGF
no EGF
EGF + AG1478
D
Luciferase activity (% of mock peak)
Time normalized to EGF peak (hours)
EGF
PMA
B
Luciferase activity (% of mock peak)
Time normalized to mock peak (hours)
mock siRNA
EGFR KD
E
Luciferase activity (% of mock peak)
Time normalized to mock peak (hours)
mock siRNA
MEK1+2 dKD
C
Luciferase activity (% of mock peak)
Time normalized to GFP peak (hours)
GFP
GFP-EGFR
F
Luciferase activity (% of mock peak)
Time normalized to EGF peak (hours)
EGF
EGF + U0126
G
no EGF
15 min EGF
15 min EGF & AG
15 min PMA
15 min PMA & AG
EGFR
P-EGFR
P-MEK1/2
P-ERK1/2
MEK1/2
H
mock siRNA
EGFR KD
EGFR
MEK1+2
SNX3
I
GFP
GFP-EGFR
GFP-EGFR
EGFR
TSG101
GFP
J
mock siRNA
MEK1+2 KD
HRS
MEK1+2
RAB5

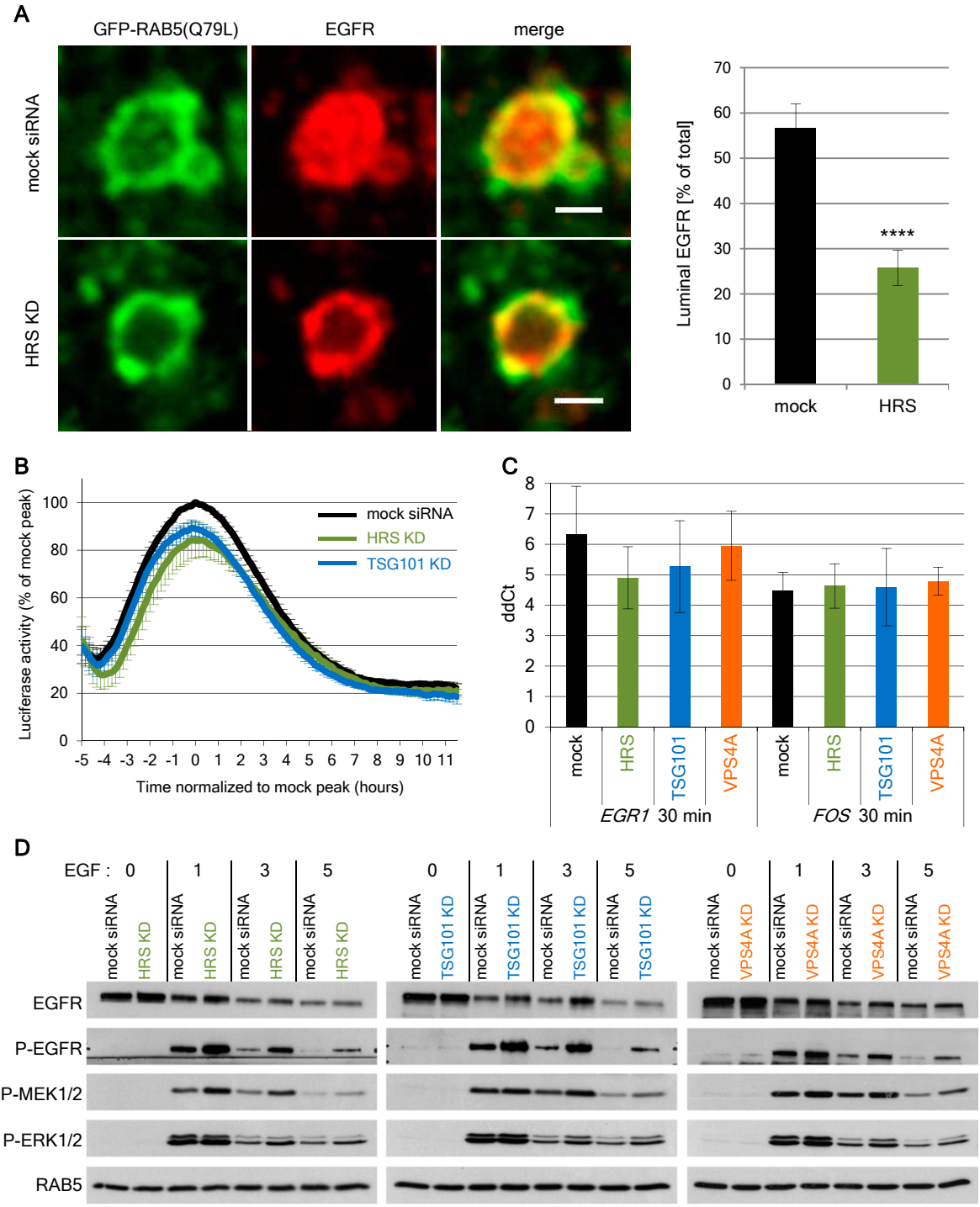
A
GFP-RAB5(Q79L)
EGFR
merge
mock siRNA
HRS KD
Luminal EGFR [% of total]
70
60
50
40
30
20
10
0
****
mock
HRS
B
Luciferase activity (% of mock peak)
100
80
60
40
20
0
mock siRNA
HRS KD
TSG101 KD
-5 -4 -3 -2 -1 0 1 2 3 4 5 6 7 8 9 10 11
Time normalized to mock peak (hours)
C
ddCt
8
7
6
5
4
3
2
1
0
mock
HRS
TSG101
VPS4A
mock
HRS
TSG101
VPS4A
EGR1 30 min
FOS 30 min
D
EGF : 0 1 3 5
mock siRNA
HRS KD
TSG101 KD
VPS4A KD
EGFR
P-EGFR
P-MEK1/2
P-ERK1/2
RAB5

Brankatschk - Fig. 3

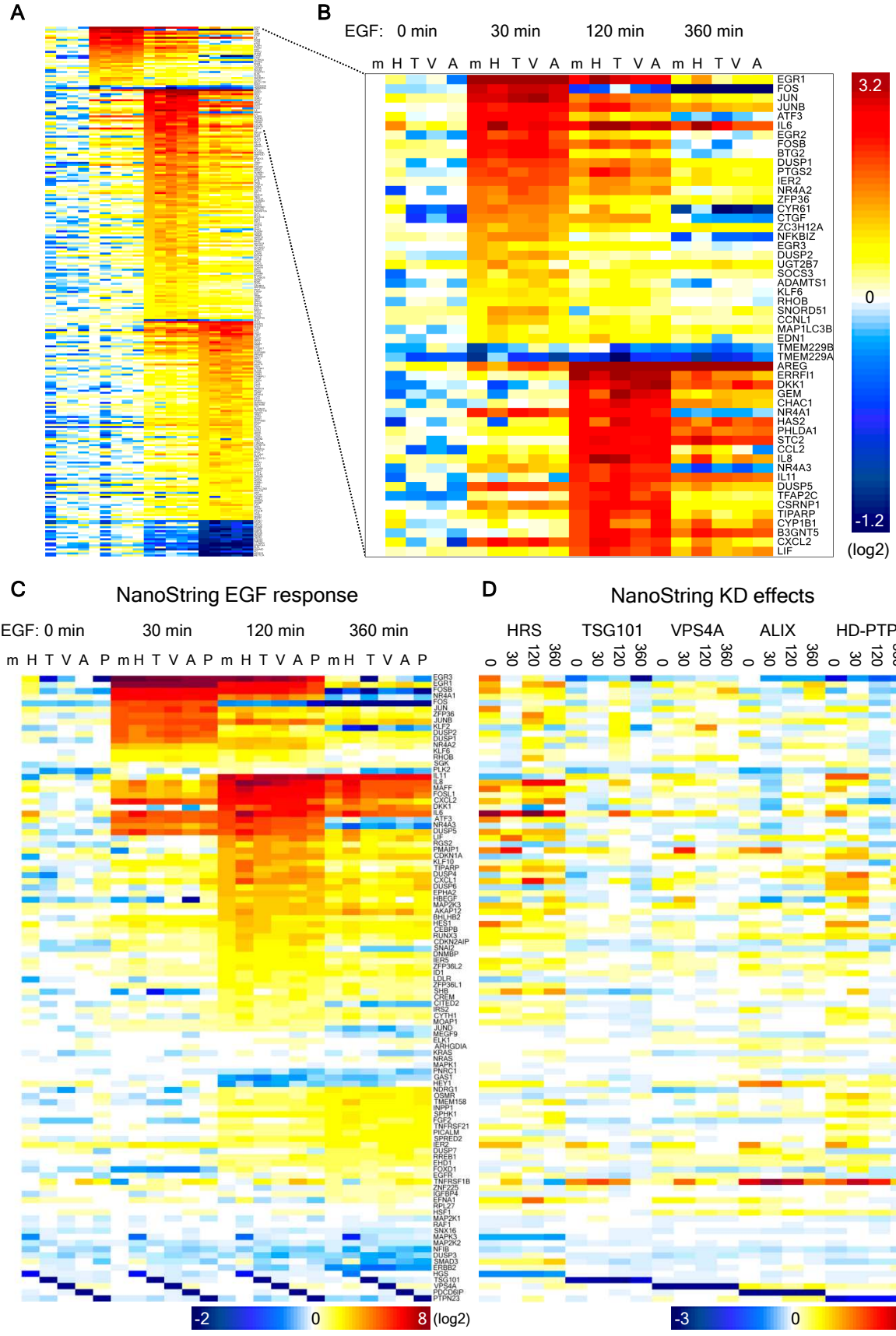

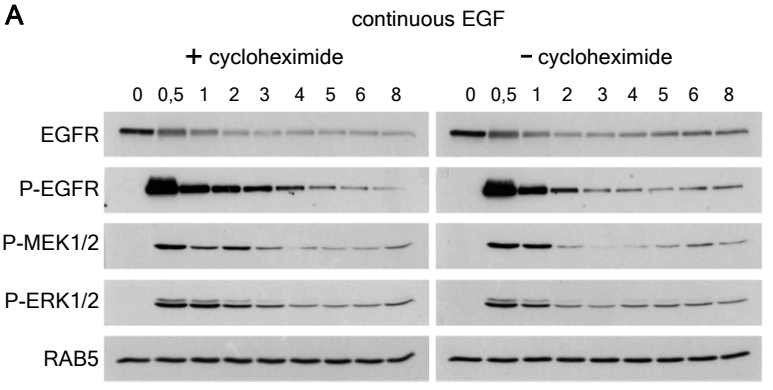
A
continuous EGF
+ cycloheximide
− cycloheximide
0 0,5 1 2 3 4 5 6 8
0 0,5 1 2 3 4 5 6 8
EGFR
P-EGFR
P-MEK1/2
P-ERK1/2
RAB5

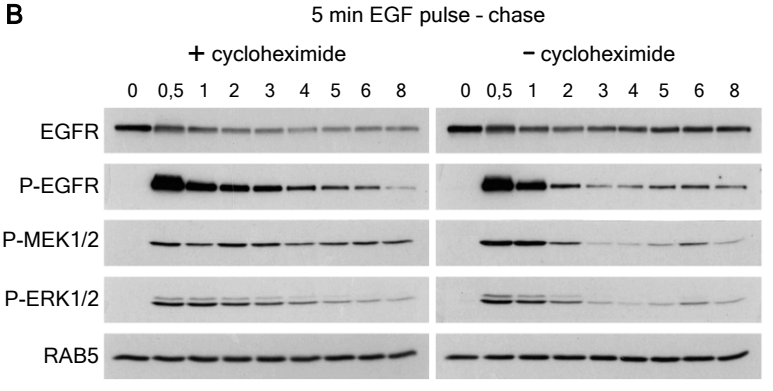
B
5 min EGF pulse - chase
+ cycloheximide
− cycloheximide
0 0,5 1 2 3 4 5 6 8
0 0,5 1 2 3 4 5 6 8
EGFR
P-EGFR
P-MEK1/2
P-ERK1/2
RAB5

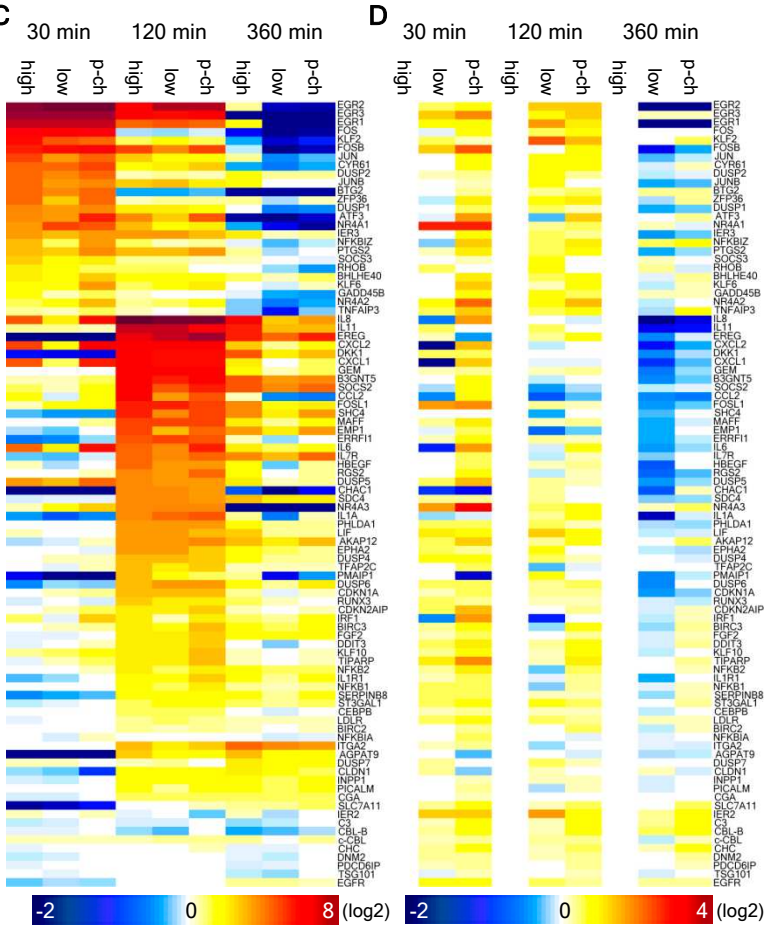
C
30 min
120 min
360 min
high
low
p-ch
high
low
p-ch
high
low
p-ch
EGR2
EGR3
EGR1
FOS
KLF2
FOSB
JUN
CYR61
DUSP2
JUNB
BTG2
ZFP36
DUSP1
ATF3
NR4A1
IER3
NFKBIZ
PTGS2
SOCS3
RHOB
BHLHE40
KLF6
GADD45B
NR4A2
TNFAIP3
IL8
IL11
EREG
CXCL2
DKK1
CXCL1
GEM
B3GNT5
SOCS2
CCL2
FOSL1
SHC4
MAFF
EMP1
ERRFI1
IL6
ILTR
HBEGF
RGS2
DUSP5
CHAC1
SDC4
NR4A3
IL1A
PHLDA1
LIF
AKAP12
EPHA2
DUSP4
TFAP2C
PMAIP1
DUSP6
CDKN1A
RUNX3
CDKN2AIP
IRF1
BIRC3
FGF2
DDIT3
KLF10
TIPARP
NFKB2
IL1R1
NFKB1
SERPINB8
ST3GAL1
CEBPB
LDLR
BIRC2
NFKBIA
ITGA2
AGPAT9
DUSP7
CLDN1
INPP1
PICALM
CGA
SLC7A11
IER2
C3
CBL-B
c-CBL
CHC
DNM2
PDCD6IP
TSG101
EGFR
-2
0
8
(log2)
D
30 min
120 min
360 min
high
low
p-ch
high
low
p-ch
high
low
p-ch
-2
0
4
(log2)

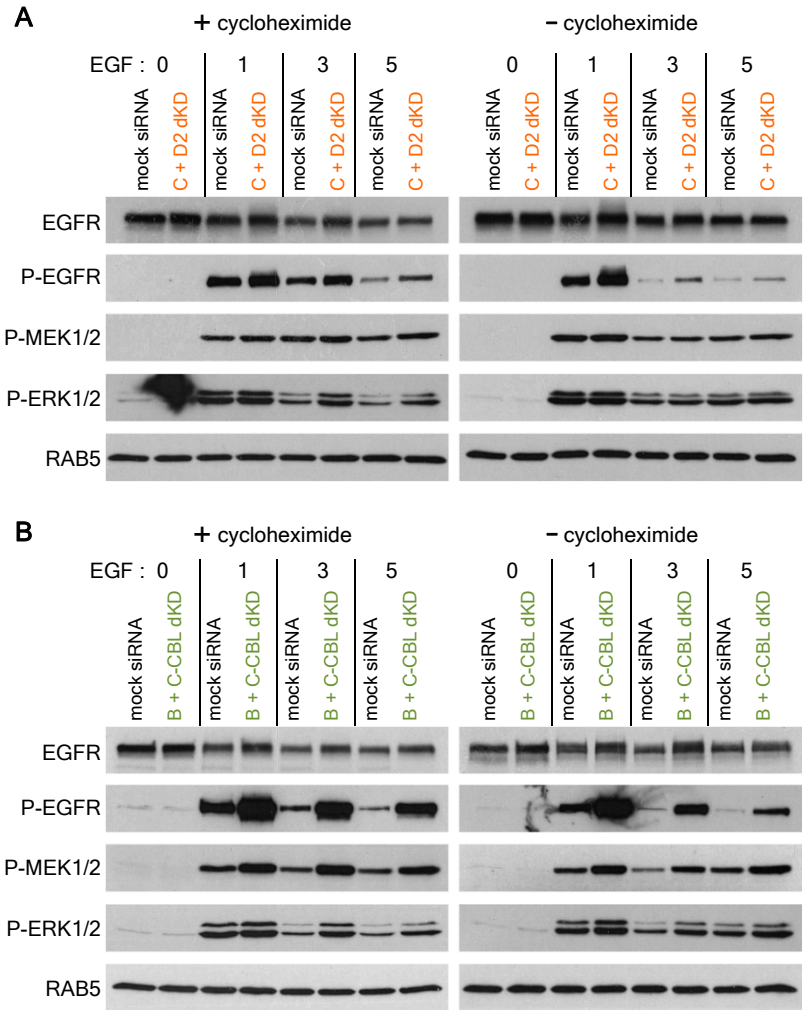
A
+ cycloheximide
− cycloheximide
EGF : 0 1 3 5
mock siRNA
C + D2 dKD
EGFR
P-EGFR
P-MEK1/2
P-ERK1/2
RAB5
B
+ cycloheximide
− cycloheximide
EGF : 0 1 3 5
mock siRNA
B + C-CBL dKD
EGFR
P-EGFR
P-MEK1/2
P-ERK1/2
RAB5

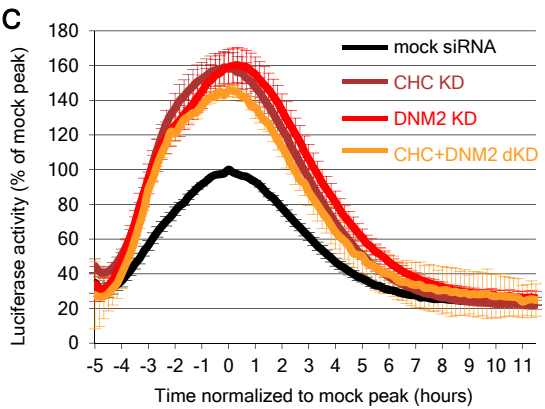
C
Luciferase activity (% of mock peak)
Time normalized to mock peak (hours)
mock siRNA
CHC KD
DNM2 KD
CHC+DNM2 dKD

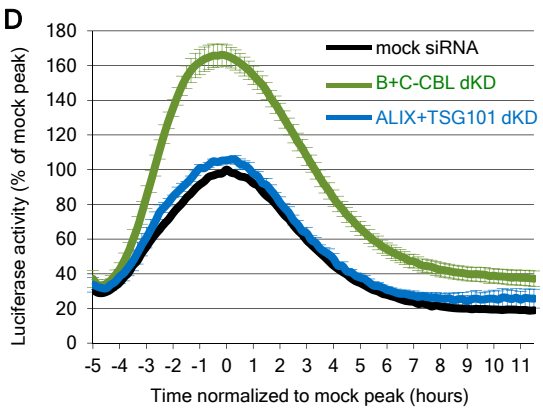
D
Luciferase activity (% of mock peak)
Time normalized to mock peak (hours)
mock siRNA
B+C-CBL dKD
ALIX+TSG101 dKD

Brankatschk - Fig. 6

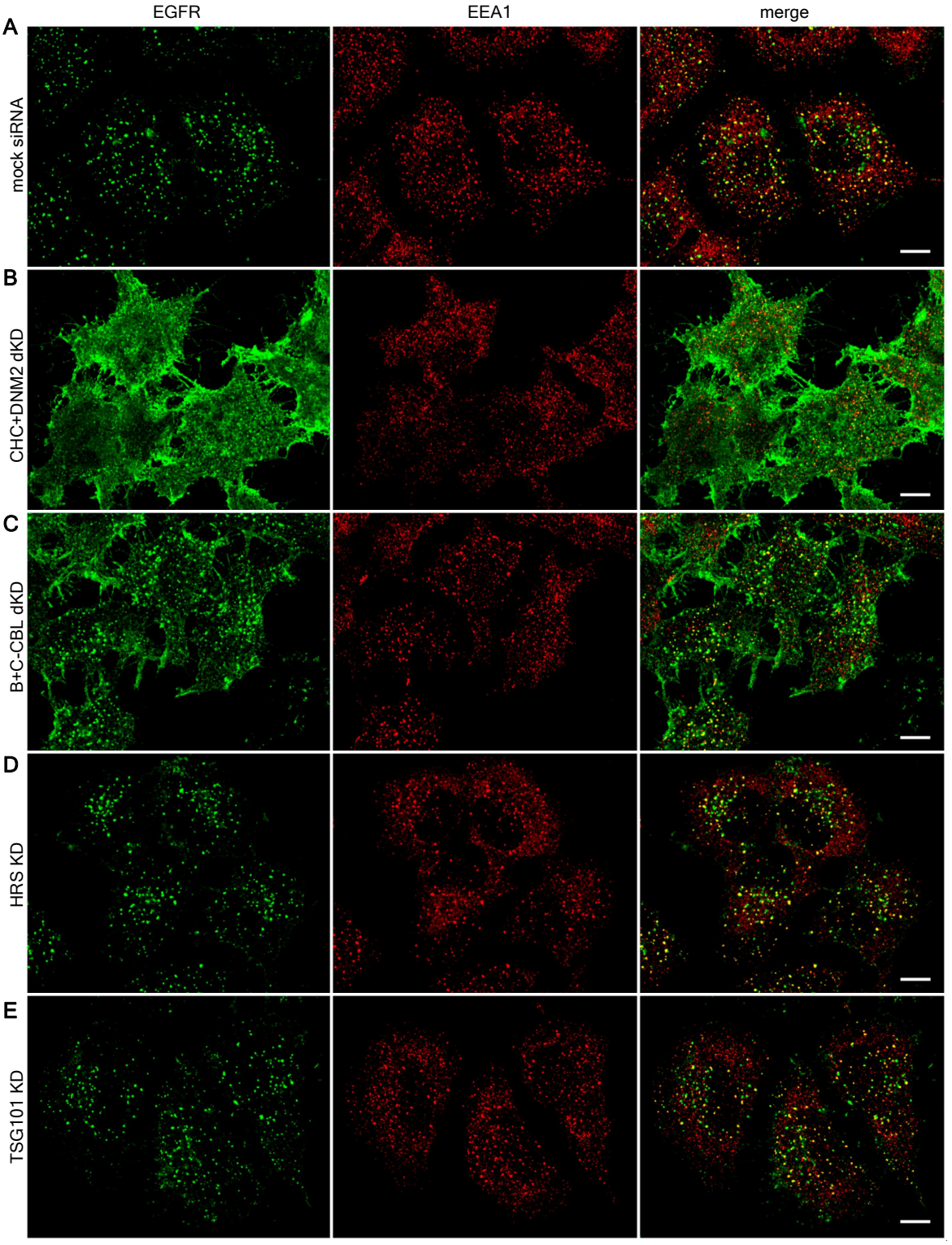

Brankatschk - Fig. 7